Long-term geomechanical behavior of geogrid-reinforced ballast in dynamic triaxial tests

Lucas Machado de Souza[1#] (iD), Paulo César de Almeida Maia[1] (iD),

Maria Cecília Martins Gomes Rangel[1] (iD)

Article

Keywords

Cubic particle
Cyclic triaxial tests
Geogrid stiffness
Geosynthetics reinforcement
Plastic deformation

Abstract

During operation, the ballast is subjected to a gradual breakage process that causes clogging of the substructure. Intervention periods on the ballast layer generate high costs that impact the long-term competitiveness of railways. In this context, this work aims to evaluate the geomechanical behavior of reinforced ballast, assessing the effect of reinforcement and stiffness provided by the addition of geogrids. Using 3D printing, the two reinforcement elements were manufactured with PETG and PLA polymers to represent the commercial geogrids Basetrac Grid PET40 and PET65, respectively. Long-term cyclic triaxial tests were used to evaluate the geomechanical behavior of the ballast. The results show that the PLA polymer was more efficient in reducing the deformability of the ballast. Long-term tests also demonstrated that granular materials tend to stabilize plastic deformations, which were not achieved under the stress level and loading frequency adopted in this research, even with the inclusion of geogrids. The low degree of grain breakage shows that the use of cubic particles, together with a well-graded distribution, helps to reduce aggregate degradation in the ballast layer. However, the high confinement levels used in the triaxial tests may have reduced the effect achieved by the reinforcement element. Factors associated with the model geogrids, such as high stiffness, low flexibility, and reduced aperture, also influenced the interaction with the aggregates.

1. Introduction

The railway track is one of the most important transportation systems worldwide, providing a surface that allows trains to transport passengers and loads by a set of two parallel rows of rails, which are located above the substructure, composed of ballast, subballast and subgrade. Ballast particles should resist vertical and longitudinal forces, hold track position, provide water drainage, prevent vegetation growth, provide energy absorption for the track and reduce permanent settlement.

During life span, ballast layer, submitted to cyclic loads, shows an elastoplastic response under traffic loading characterized by a recoverable deformation, due to the compaction process, and a permanent deformation, due to breakage of particles (Lekarp et al., 2000; Anbazhagan et al., 2012). Unlike elastic or residual deformation, the accumulation of plastic deformations is important to predict long-term behavior and understanding the failure mechanisms of granular materials.

Under cyclic loading, ballast particles gradually change in shape, size and compressibility because of attrition and breakage

over time, resulting in the formation of fines and contributing to track settlement (Sun et al., 2016). Werkmeister et al. (2001) improved the concept of shakedown and divided the geomechanical behavior of granular materials into three phases: elastic shakedown, plastic shakedown or creep and failure. On elastic shakedown stage, the permanent strain would eventually stabilize in response to cyclic loading, achieving a state of shakedown after the compaction period, which is acceptable to railroad. On creep stage, the permanent strain doesn't stabilize, remaining constant after the compaction period. On failure stage, poor track performance caused by excessive settlement leads the railroad to collapse.

The degradation of railways requires maintenance operations based on the track geometry to renew structure and improve the bearing capacity, because track performance is predominantly related to the ballast layer. Fine particles derived from degradation and other sources accumulate in the ballast layer in a process known as fouling. Under these conditions, the ballast loses its functional capacity over time, decreasing shear strength and drainage capability, leading to increase maintenance costs (Anderson & Fair, 2008; Huang et al., 2009; Indraratna et al., 2014; Koohmishi &

Soil. Rocks, São Paulo, 2025 48(2):e2025008924

1

Palassi, 2018). Over the years, railway projects have focused on the superstructure, which includes rails, fasteners and sleepers, due to the complexity of the parameters that influence the geomechanical behavior of granular materials. However, the costs associated with interventions on the ballast layer represent more than 70% of the total cost of the corrective maintenance process (Sgavioli et al., 2015). In addition, the demand for high-speed transport has grown in the last years, increasing densification on existing tracks.

Substructure reinforcement with geosynthetics presents an alternative method to reduce lateral spread and to enhance track performance, compared to standard corrective maintenance solutions such as tamping, stoneblowing, and ballast cleaning. Although tamping has been widely used for railway maintenance, being the most effective way of correcting geometry faults, this process causes a reversion to its previous track geometry with further repeated traffic loading by a phenomenon known as ballast memory. Eventually, the time between maintenance cycles becomes shorter and the grains must be replaced or cleaned again. Created to prevent ballast memory, stoneblowing is a technique that blows smaller stones below the sleeper without disturbing particles. However, this technique doesn't correct irregularities in the track and is considered a complementary solution to tamping (Guo et al., 2021).

In recent years, several authors have conducted studies about the inclusion of geogrids in ballast to improve its lateral stability and reduced track settlement (Tutumluer et al., 2009; Chen et al., 2013; Indraratna et al., 2013; Liu et al., 2016; Sweta & Hussaini, 2020). Geogrids are flat synthetic structures composed of longitudinal and transverse filaments, characterized by high tensile strength. The reinforcement element increases grain confinement and reduces lateral movement through a mechanism known as interlocking (Fernandes et al., 2008; Shukla et al., 2009; Abu-Farsakh et al., 2012; Palmeira et al., 2021; Desbrousses et al., 2023). However, despite the great improvement from this solution, the interaction between granular materials and geogrid is highly complex and challenging.

In consequence, understanding the reinforcement influence on geomechanical behavior of ballast settlement is vital to optimizing maintenance costs. Researchers around the world have been conducting studies under laboratory conditions to meet future requirements of heavy traffic and optimize the railroad life span (Suiker et al., 2005; Lackenby et al., 2007; Merheb et al., 2014; Delgado et al., 2019). Dynamic triaxial tests or Repeated Load Tests (RLT) may simulate in laboratory a stress state with confinement and deviator stress over granular particles.

On RLT, the axial load is programmed as a sinusoidal pulse, which is composed of a load period followed by a short rest period. The constant confining pressure simulates the mean pressure due to geostatic stress in the field and each vertical load applies a pulse to simulate the effect of the train wheel. This procedure is used to evaluate elastic behavior by resilient tests and plastic behavior by permanent deformation or long-term tests.

However, despite the previous studies about the geogrid reinforcement of the ballast layer using RLT, the long-term geomechanical behavior of the aggregates is not fully known, because it is influenced by intrinsic and extrinsic factors which commit stress state representation and boundary conditions (Sun et al., 2016; Sweta & Hussaini, 2020; Alabbasi & Hussein, 2021). In this respect, the evaluation of the geomechanical behavior of the ballast involves field or laboratory procedures which are focused on the characteristics of interest, eliminating second-order effects associated with the remaining characteristics. Only in this way it is possible to determine the effect of each characteristic individually. For this purpose, this paper evaluated ballast reinforcement on small-scale samples using cubic cementitious particles to emphasize the effect of geogrid.

2. Materials and methods

2.1 Granular materials

Characterized by enhanced packing density, UHPC (Ultra-high Performance Concrete) presents superior durability compared to conventional concrete. In fact, UHPC is composed of fine materials, with optimized grading curves, microfibers, and a low water-cement ratio. Following these characteristics, all particles were produced using a type V Portland cement and rice husk ash as cementitious materials. Following the mix proportions established by Conceição et al. (2022) (Table 1), ground quartz, two quartz fine sands and wollastonite fiber were used as filler, fine, and micro-reinforcement, respectively.

Gneiss particles (medium-grained rock) were used as the natural railway ballast aggregate for comparison with UHPC. This metamorphic rock has a compressive strength of 124 MPa obtained from 50 mm cubic specimens and it was collected in the city of Itaperuna in Rio de Janeiro state, Brazil. Every particle has a cubic shape previously cut on a table saw.

The gradation No. 24, proposed by American Railway Engineering and Maintenance-of-Way Association (AREMA,

Table 1. Proportions of UHPC for 1 m³.

Material	Mass, m (kg)	Density, ρ (g/cm³)
Cement	1013.0	3.10
Rice husk ash	53.3	2.09
Ultrafine quartz	81.6	2.65
Fine sand (150 μm)	61.0	2.65
Fine sand (425 μm)	832.0	2.65
Wollastonite	76.7	2.90
Superplasticizer	51.3	1.21
Water	196.1	1.00

2

Soil. Rocks, São Paulo, 2025 48(2):e2025008924

2015), which is used on heavy haul tracks around the globe under a long-term loading, with a reduction factor of 3.5, was adopted as a reference for grain size distribution of the ballast (Figure 1) due to widespread use on heavy haul railways. Delgado et al. (2019) also explain that this gradation also provides good interlocking between grains.

All particles (19.0 to 4.76 mm) were produced in a cubic shape with roughly rounded corners (Figure 2). The cubic shape reduces the breakage during loading and centralizes the influence of reinforcement element on ballast, eliminating second-order factors on geomechanical behavior like strength, lithological and morphological characteristics of rock.

Ballast production was divided into three phases: mixture, curing and polishing. During the first phase, a paint mixer attached to a column drill was used to achieve the required workability of the concrete. The aggregates in silicone molds were demolded after 48 hours and remained in curing on water for 28 days. Then, all aggregates stayed at the Micro-Deval for 20 minutes to complete the polishing of edges. Along with the small particles, three 50 mm specimens were also produced following the same process on a concrete vibrating table to evaluate compressive strength.

In accordance with ASTM D6928 (ASTM, 2017) and ASTM C127 (ASTM, 2015), UHPC aggregates were characterized for compressive strength, Micro-Deval

abrasion, relative density and water absorption, respectively. For compressive strength, the three specimens of 50 mm were tested in a servo-hydraulic universal machine with a displacement rate of 0.5 mm/min. Using the caliper, the edges of the three samples were measured to the calculation of the cross-sectional area. For Micro-Deval abrasion resistance, a 1.5 kg sample (from 6.2 to 12.0 mm) was placed in a steel jar mill and rotated for 2 hours with 2 L of water and 5 kg of steel balls with 9.5 mm of diameter. Subsequently, the particles were washed and separated from the abrasive charges. All material retained on sieve #16 (1.18 mm) was dried in an oven at a temperature of (110 ± 5) °C. As presented in Equation 1, the abrasion loss (M_{de}) was determined from the relationship between the dry mass before (m_a) and after the test (m_b). For relative density and water absorption, six 19.0 mm particles were soaking in water to obtain submerged mass, dried in air to obtain saturated mass and dried on stove for 48 hours to obtain dried mass.

$$M_{de} \ (\%) = \frac{m_a - m_b \ (kg)}{m_a \ (kg)} \ x \ 100 \qquad (1)$$

2.2 Geogrids

Manufactured with polymers PET (Polyethylene Terephthalate) or PP (Polypropylene), Basetrac Grid is a group of geogrids of high flexibility and strength utilized for roadways and railway reinforcement. The biaxial geogrids PET40 (40 kN/m tensile strength) and PET65 (65 tensile strength) (Figure 3) were chosen as reference for the confection of geogrids model X (more flexible) and model Y (more rigid) to evaluate the effect of reinforcement on the long-term geomechanical behavior and stiffness on the confinement level, respectively. Both geogrids have a 25 mm mesh opening and 1.0 mm filament thickness.

Tensile strength tests were conducted in longitudinal direction by a servo-hydraulic universal machine with a rate of 20 mm/min to determine the tensile strength (T), obtained from the force as a function of the sample width, and deformation in the break, by the ratio between the displacement and the
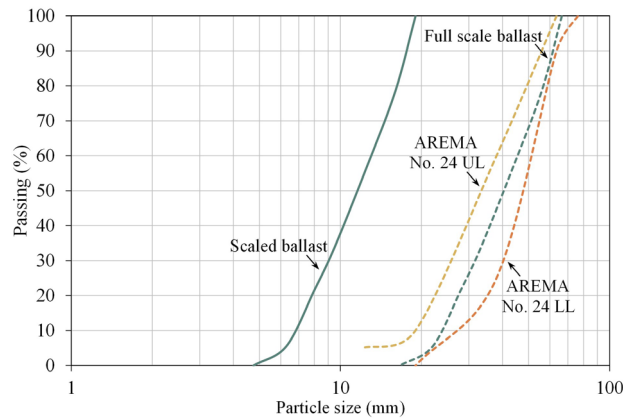
Figure 1. Particle size distribution of scaled ballast (UL: Upper Limit; LL: Lower Limit).

Figure 2. UHPC particles (19.0 to 4.76 mm).

distance between claws. Furthermore, the secant modulus (J) was determined by the ratio between resistance (T) and deformation (ε) (Equation 2).

$$J\,(\text{kN/m}) = \frac{T\,(\text{kN/m})}{\varepsilon} \qquad (2)$$

According to Brown et al. (2007) observations, grid opening, rib width and secant modulus are the most influential properties of geogrids on ballast geomechanical behavior. These three characteristics were considered as reference to create the model geogrids. Like UHPC aggregates, a reduction factor (λ) of 3.5 was initially applied to model geogrids. The scale factors followed the physical modeling studies established by Viswanadham & König (2004) for 1g models.

Developed on SketchUp (3D design software), the model geogrids have 7.0 mm of aperture, 1.7 mm of filament width and 0.3 mm of thickness. Considering scale effect of 3.5, both geogrids were manufactured by 3D impression with the polymers PETG (Polyethylene Terephthalate Glycol), a more flexible material used to create geogrid model X, and PLA (Polylactic Acid), a more rigid material used to create geogrid model Y. The polymer TPU (Thermoplastic Polyurethane) was initially tested, but it presented lower resistance and higher deformability, characteristics unsuitable for use as a reinforcing element in granular layers.

In addition to tensile tests, static puncture tests were conducted at a deformation rate of 50 mm/min. The correlation between tensile force (F) and piston radius (r_p), proposed by Cazzuffi et al. (1986) (Equation 3), was also used to determine the tensile strength (T).

$$T\,(\text{kN/m}) = \frac{F\,(\text{kN})}{2\,\pi\,r_p\,(\text{m})} \qquad (3)$$
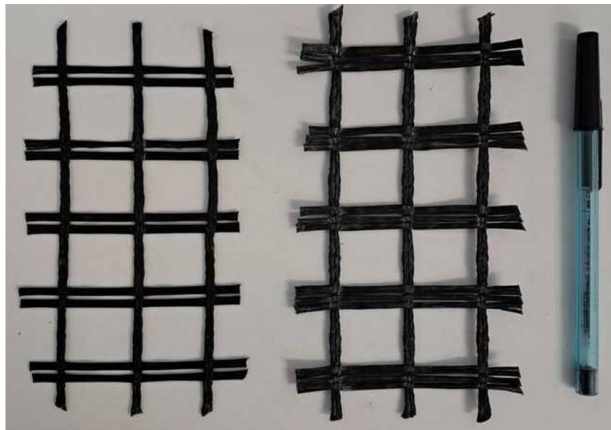
2.3 Sample preparation and testing

Three cyclic loading tests were conducted on cylindrical specimens (20 cm in height and 10 cm in diameter), with a density of 1 g/cm³, to evaluate the contribution of geogrid in the permanent deformation. The first test (PD-I) was performed without reinforcement inclusion. The second (PD-II) and third tests (PD-III) were conducted with geogrids PETG and PLA, respectively. Both geogrids were positioned at 1/3 of bottom of the specimen. Several authors recommend a ratio between the maximum particle size and diameter of the specimen for scale effects to become negligible. Skoglund (2002) suggests values between the range 1/5 and 1/7 while the standard ASTM D5311 (ASTM, 2011) specifies a maximum ratio of 1/6. Following the recommendations, the ratio adopted was equal to 1/5.2.

During the preparation of the sample, PVC (Polyvinyl Chloride) flexible strips (220 mm in height, 15 mm in width, and 2 mm in thickness) were fixed at the lower cap. A latex membrane (0.4 mm thickness) was attached to the specimen, filled with cubic aggregates. At bottom of triaxial cell, a drain was connected to a vacuum pump to eventually check the presence of holes in membrane and prevent the occurrence of deformations on the sample before starting the tests. Next, a top cap was placed, and rubber O-rings were used to fix the membrane and seal the sample. Finally, a second membrane was used to cover the specimen (Figure 4). The values of displacement were obtained by two axial LVDT (Linear Variable Differential Transducer) installed around the sample. The use of three transducers to measure axial deformations, as recommended in literature, was not possible to implement considering the limitations of the data acquisition system.

Figure 3. Geogrids Basetrac Grid PET40 and PET65.
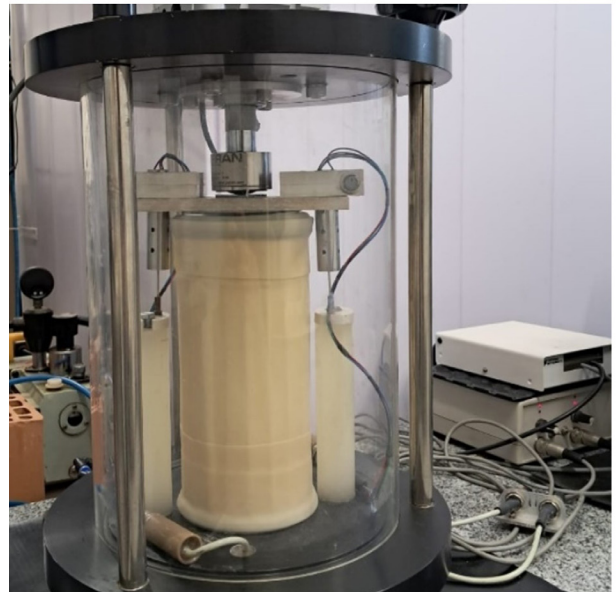
Figure 4. Specimen on triaxial chamber test.

4

Soil. Rocks, São Paulo, 2025 48(2):e2025008924

Inside the triaxial cell, constant confinement stress was applied by compressed air. Deviatoric stress was repeated and applied using a vertical load provided by a 5 kN load cell connected hydraulically to an actuated piston and pneumatic system. The use of this load cell was appropriate for reduced-scale testing proposed in this research, considering its stainless-steel body, high resistance to vibrations and compact size.

Isolated tests conducted on the sample to analyze the membrane effect showed a correction of 12% for a confinement stress of 1 kPa. Indraratna et al. (1998) observed a correction of 8% for the same stress state and membrane. Although, Shi (2009) explains that membrane effect correction is negligible on tests conducted in dry conditions.

All single-stage permanent deformation tests were conducted in a single stage, corresponding to a heavy haul railway with 32.5 tons per axle, maximum speed of 80 km/h and 4 m distance between bogies. The deviator stress was estimated with empirical equations used by Delgado et al. (2019). Considering freight trains, the stress state adopted was 70 kPa for confinement stress and 280 kPa for cyclic deviator stress, with a frequency of 2 Hz and one million loading cycles. Lower frequencies, such as 1 to 3 Hz, commonly used on repeated load tests, do not affect significantly the permanent strain (Zhang et al., 2019).

A sinusoidal pulse, composed of a 100 ms (0.1 s) loading period followed by a 400 ms (0.4 s) rest period, was applied to the specimen. Figure 5 shows the load pulse applied during the repeated load test conducted in this current study. Due to data acquisition system limitations, readings were made at each 50,000 cycles for the first 250,000 cycles, 350,000 cycles, 450,000 cycles, 550,000 cycles, 700,000 cycles, and one million cycles. Therefore, the readings didn't follow standard EN 13286-7 (EN, 2004) recommendations.

This loading pattern pulse is a simplification designed for laboratory studies. In fact, three axles, corresponding to the wheelset rail, should be considered to represent correctly the railway cyclic loading, providing a more realistic and accurate prediction of the long-term geomechanical behavior of ballast (Jideani & Gräbe, 2020).

Despite the limitations of the triaxial system software used in this research, it was possible to observe the test configurations, such as the stress state, transducer readings, total number of cycles, real-time cycle and the load pulse.

After each test, the fines were sieved to evaluate the grain breakage, which was analyzed by index B_g (Grain Breakage) (Marsal, 1967). The index B_g (Equation 4) was

calculated as a summation of positive values of the difference in percentage by mass of particles retained on each sieve before (W_{ki}) and after triaxial test (W_{kf}). The index *BBI* (Ballast Breakage Index) (Indraratna et al., 2005) was calculated with the correlation established by Hussaini (2013) presented in Equation 5.

$$B_g\ (\%) = W_{ki} - W_{kf}\ (\%) \tag{4}$$

$$B_g\ (\%) = 0.25 BBI\ (\%) + 0.32 \tag{5}$$

3. Results and discussions
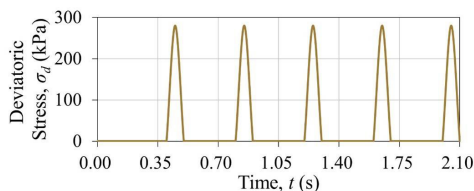
3.1 Characterization of aggregates

The properties of UHPC and gneiss aggregates are available on Table 2. Compared to the physical and mechanical properties of the UHPC aggregates from Conceição et al. (2022), the particles from this research were significantly more porous (58.7% higher), even though the mix proportions were identical. These differences in physical properties are associated with the adverse reaction caused by the additive used in this study during the curing process. The effect can also be observed in the loss by abrasion in the Micro-Deval test (62.3% higher). This superficial loss was not observed in the particles produced for the characterization tests, although the layer was formed. However, it should be noted that, exceptionally, during the molding of the particles, for the physical and mechanical characterization tests, a concrete vibrating table was used. The other particles were molded only using a spatula over a bench.

Despite these differences, the compressive strength (σ_{cs}) achieved was very close to Gneiss (3.71% lower), attending to the minimum limit of 120 MPa requested by ASTM C1856 (ASTM, 2024) for a UHPC material. In addition, water absorption (α) and aggregate density (ρ) could be easily controlled by proportions and the use of other types of additives, which is a significant advantage of concrete over natural rock.

Figure 5. Load pulse in permanent deformation test.

Table 2. Characteristics of particles.

Properties	Result of this study	UHPC*
Density, ρ (kg/m³)	2330.03	2673.98
Porosity, η (%)	7.3	4.6
Water absorption, α (%)	3.1	1.9
Micro-Deval abrasion, M_{de} (%)	20.5	12.63
Compressive strength, σ_{cs} (MPa)	119.66	132.3

*According to Conceição et al. (2022).

3.2 Characterization of geogrids

During tensile tests on model geogrids, slippage was observed during loading due to the smooth texture of the printed material compared to rough surface of prototype geogrids. This slippage increased the displacements measured by the system, leading to errors in the stress-strain curves. To solve this issue, a low grit sandpaper was added to the front clamping jaws.

In addition, both PETG and PLA polymers showed a high stiffness (J) compared to PET used on Basetrac Grid geogrids. Consequently, ribs of the geogrid were breaking during the fitting into the grips, even without any application of pre-load. Therefore, the thickness (c) of the material was changed from 0.3 mm to 0.6 mm to continue the tests. All properties from model and prototype geogrids are available in Table 3.

Considering a scale factor of 3.5 squared for secant stiffness proposed by Viswanadham & König (2004) for 1g models, it was observed that PETG and PLA model geogrids exhibited higher stiffness compared to the Basetrac Grid PET40 and PET65 geogrids. Applying the scale factor on the prototype geogrids, it should be expected a secant stiffness of 33.5 kN/m for PETG and 50.5 kN/m for PLA. Thus, the results of 120.69 and 203.66 kN/m did not meet the scale factor. However, it is worth noting that the strength values of PET40 and PET65 geogrids obtained on tensile tests (29.23 and 40.10 kN/m respectively) were lower compared to the commercial specifications provided by the manufacturer (40.0 and 65.0 kN/m respectively). Figure 6 presents the final schematic representation of the model geogrids developed on SketchUp.

The static puncture tests didn't show good correlations on prototype geogrids showing 50% less strength compared to tensile tests, resulting in 14.13 kN/m for PET40 and 19.28 kN/m for PET65. On model geogrids, the correlations resulted in 1.52 kN/m for PETG, following the tendency on prototype geogrids, and 0.97 kN/m for PLA, being the worst correlation with a strength 76.4% lower.

3.3 Permanent deformation tests

During the first 350,000 cycles, increments of plastic deformation were higher due to the stabilization process

of axial deformations under the applied stress level. The ballast undergoes significant initial deformations due to grain movement, which promotes wear between the particles. In all tests, the material exhibited a tendency to stabilize, even without the inclusion of geogrid (Figure 7). This behavior was also observed by Indraratna & Salim (2003), Abu-Farsakh et al. (2007), Indraratna et al. (2010), and Qian et al. (2018). However, unlike the cited studies, plastic deformations did not reach the shakedown point. Even after reaching one million cycles, the deformations kept a tendency of growth.

All tests were executed with pauses every 50,000 cycles during the first 350,000 cycles. It should be noted that conditioning of the sample between readings may have influenced these results, considering that particles have shown a tendency of stabilization at the first 100,000 cycles based on other studies. This procedure was limited by the data acquisition system and software employed in this research, allowing the measurement of deformations only at the end
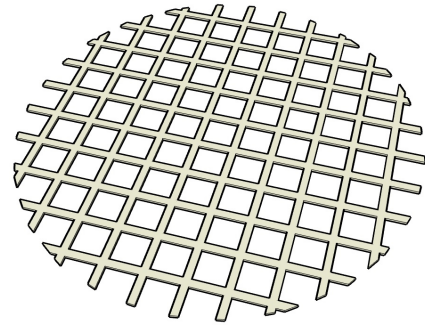

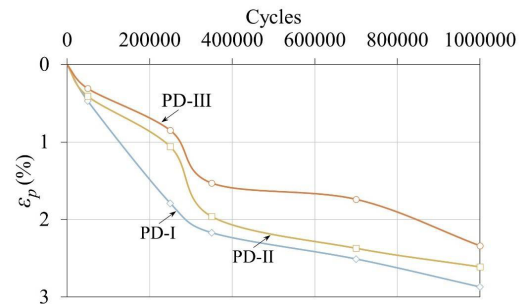**Figure 6.** Perspective of model geogrid

Figure 7. Permanent deformation *vs.* cycles.

Table 3. Characteristics of prototype and model geogrids from tensile tests.

Properties	PET40	PET65	PETG	PLA
Geogrid aperture, a (mm)	25.0	25.0	7.0	7.0
Rib width, b (mm)	6.0	6.0	1.7	1.7
Rib thickness, c (mm)	1.0	1.0	0.6	0.6
Tensile strength, T (kN/m)*	29.23	40.10	2.86	4.11
Deformation, ε (%)*	7.12	6.47	2.37	2.02
Secant stiffness, J (kN/m)*	410.35	619.80	120.69	203.66

*On machine direction (MD).

cycle count, despite the procedure of 20 continuous readings for the first 20 cycles from standard EN 13286-7 (EN, 2004). Then, it was not possible to estimate the effect of deviatoric stress on plastic behavior because the long-term tests were limited by one stress state. Furthermore, the RLT doesn't allow to simulate the principal stress rotation, therefore, it was not viable to simulate the reversal of shear stress.

Geogrid PETG reduced a maximum deformation of 40.8% while geogrid PLA reduced to 52.5% (Figure 8). These results showed an influence of reinforcement effect and stiffness on the deformation of granular materials. Nevertheless, the ratio between the geogrid aperture size and the average particle diameter (a/d_{50}) used in this study was 0.6, which is considered a feeble interlocking zone (McDowell et al., 2006; Indraratna et al., 2013; Han et al., 2018). This observation corroborates the studies of Brown et al. (2007), proving that geometric parameters of the geogrid, such as aperture size and secant stiffness, may influence the deformability of the ballast layer. Abu-Farsakh et al. (2007) also recognized the influence of geogrid arrangement. However, this effect cannot be analyzed considering that the tests only used one geogrid for each specimen.

Commercial geogrids such as Basetrac Grid are rigid, but they exhibit a high level of flexibility in interaction with the ballast particles. This behavior was not observed in the model geogrids PETG and PLA during characterization and triaxial tests. The alignment of the fibers in these polymers combined with the smooth texture contrasts with the rough surface of the prototype geogrids PET40 and PET65. Nonetheless, it should be noted that the high level of confinement (70 kPa) has influenced the interlocking mobilized by the reinforcement element.

As observed in Figure 9, the polymers exhibit high stiffness and low flexibility between filaments and junctions. The deformability of the components is more noticeable in PETG, due to its lower rigidity. It should be noted that the deformation presented in one of the PLA filaments may be associated with the ballast compaction process on PD-III test.

Compared to the granite aggregates submitted to one million cycles evaluated by Delgado et al. (2019), the degradation of UHPC particles without geogrid inclusion was 36.46% lower considering B_g index (2.30% against 3.62%). However, the triaxial tests conducted in this research were performed using a controlled form of ballast. Therefore, the shape control of the aggregate, together with the use of a uniformity coefficient (C_u) close to 2.0 (1.91), as Indraratna et al. (2006) and Shi et al. (2023) recommend, contributed to reducing material breakage, even without addition of the reinforcement element (Table 4).
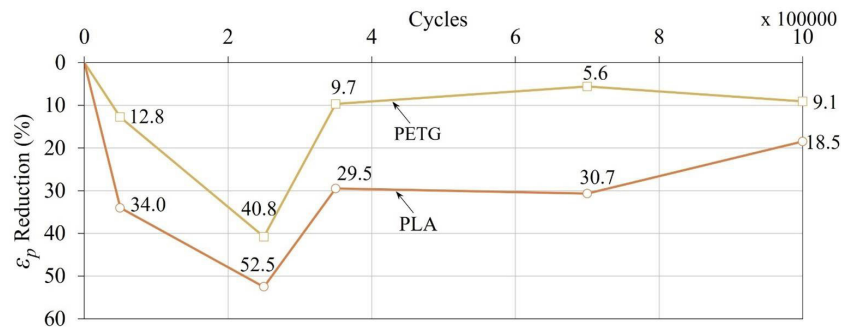
Figure 8. Geogrid action on long term behavior.
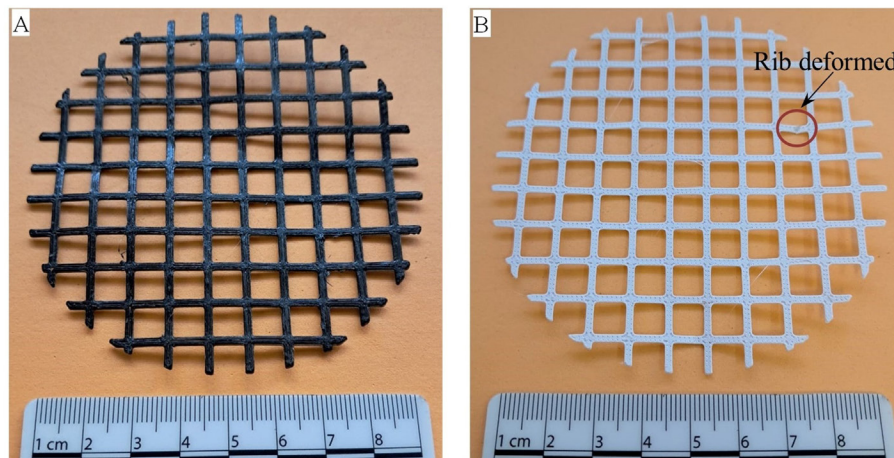
Figure 9. Model geogrids condition after long-term tests: (A) Model X (PETG) and (B) Model Y (PLA).

Soil. Rocks, São Paulo, 2025 48(2):e2025008924

7

Table 4. Particle breakage.

Index	PD-I	PD-II	PD-III
B_g (%)	2.30	2.25	2.18
BBI (%)	7.92	7.72	7.44

Based on the previous results, it is highlighted that the long-term effects of the reinforcement elements were influenced by scale factor, stiffness of the PETG and PLA polymers, and stress state. Therefore, further studies with a lower confinement level should be conducted on cubic ballast particles to observe the recurrence of this behavior. Furthermore, geogrids with larger apertures should be used to meet the spacing requirements of the interface factor recommended in the literature, with a ratio of a/d_{50} situated between 1.2 and 1.4, providing an optimum interlocking zone instead of a feeble interlocking zone. Moreover, it should be tested other model geogrids manufactured with more flexible materials to achieve better interaction with the ballast aggregates, simulating an interlocking effect closest to commercial geogrids. In addition, future studies to evaluate the effect of interlocking on radial deformations and the geomechanical behavior on multiple-stage tests may be also executed to extend the conclusions observed in this research.

4. Conclusion

Dynamic triaxial tests were conducted to evaluate the long-term geomechanical behavior of ballast. This paper investigated and evaluated the effect of reinforcement on settlement and the influence of stiffness at grain confinement provided by the addition of geogrids. For this purpose, UHPC cubic particles with slightly rounded corners, produced with a scale factor of 3.5 applied on graduation No. 24 from AREMA, were used in repeated load tests, with and without the addition of reinforcement. The methodology used on RLT aimed to simulate dynamic vertical loading from a simplified pulse. Based on experimental program developed in this research, the following conclusions can be drawn:

1. High plastic deformations were observed on aggregates during initial cycles. This behavior shows that granular materials undergo a stabilization process of permanent deformations when they are close to reaching shakedown condition;

2. The interlocking effect, promoted by the geogrid, is more noticeable during initial cycles when grains rearrange due to reinforcement elements until reaching an equilibrium state, where deformations stabilize. Besides, higher confinement levels used on repeated load tests have reduced the effect promoted by geogrids;

3. Despite the tendency to reduce plastic deformations, the shakedown condition was not reached by the ballast, even when subject to a single stress state;

4. High stiffness and smooth texture present in PETG and PLA polymers inhibited the degree of adaptability and contact with aggregates, while mesh aperture influenced the mobilization of interlocking. Therefore, geogrids exhibited partial interaction flexibility with granular material composing the ballast.

Acknowledgements

Declaration of interest

The authors have no conflicts of interest to declare. All co-authors have observed and affirmed the contents of the paper and there is no financial interest to report.

Authors' contributions

Lucas Machado de Souza: conceptualization, data curation, methodology, visualization, validation, writing – original draft & editing. Paulo César de Almeida Maia: funding acquisition, project administration, methodology, supervision, validation, resources, writing – review & editing. Maria Cecília Martins Gomes Rangel: data curation, investigation, writing – editing.

Data availability

Research data is only available upon request.

Declaration of use of Generative Artificial Intelligence

This work was not prepared with the assistance of Generative Artificial Intelligence (GenAI).

List of symbols and abbreviations

a	Geogrid aperture
b	Geogrid rib width
c	Geogrid rib thickness
d_{50}	Average particle diameter
m	Particle mass
m_a	Particle dry mass before Micro-Deval abrasion test
m_b	Particle dry mass after Micro-Deval abrasion test
r_p	Piston radius
t	Time
$vs.$	Versus

AREMA American Railway Engineering and Maintenance-of-Way Association
ASTM American Society for Testing and Materials
BBI Ballast Breakage Index
B_g Grain Breakage
C_u Uniformity coefficient
EN European Standard
F Tensile force
FAPERJ Fundação Carlos Chagas Filho de Amparo à Pesquisa do Estado do Rio de Janeiro
J Secant stiffness
LL Lower Limit
LVDT Linear Variable Differential Transducer
MD Machine Direction
M_{de} Micro-Deval abrasion resistance
PD Permanent Deformation
PET Polyethylene Terephthalate
PETG Polyethylene Terephthalate Glycol
PLA Polylactic Acid
PP Polypropylene
PVC Polyvinyl Chloride
RLT Repeated Load Test
T Tensile strength
TPU Thermoplastic Polyurethane
UENF Universidade Estadual do Norte Fluminense
UHPC Ultra-high Performance Concrete
UL Upper Limit
W_{kf} Summation of positive values of the difference in percentage by mass retained on each sieve after triaxial test
W_{ki} Summation of positive values of the difference in percentage by mass retained on each sieve before triaxial test
α Water absorption
ε Deformation
ε_p Permanent deformation
η Porosity
λ Scale factor
π Pi
ρ Density
σ_{cs} Compressive strength
σ_d Deviatoric stress

References

Abu-Farsakh, M.Y., Nazzal, M.D., & Mohammad, L.N. (2007). Effect of reinforcement on resilient and permanent deformations of base course material. *Transportation Research Record: Journal of the Transportation Research Board*, 2004(1), 120-131. http://doi.org/10.3141/2004-13.

Abu-Farsakh, M., Souci, F., Voyiadjis, G.Z., & Chen, Q. (2012). Evaluation of factors affecting the performance of geogrid-reinforced granular base material using repeated load triaxial tests. *Journal of Materials in Civil Engineering*, 24(1), 72-83. http://doi.org/10.1061/(ASCE)MT.1943-5533.0000349.

Alabbasi, Y., & Hussein, M. (2021). Geomechanical modelling of railroad ballast: a review. *Archives of Computational Methods in Engineering*, 28(3), 815-839. http://doi.org/10.1007/s11831-019-09390-4.

American Railway Engineering and Maintenance-of-Way Association – AREMA. 2015). *Manual for railway engineering* (Vol. I-IV). Lanham, MD: AREMA.

Anbazhagan, P., Bharatha, T.P., & Amarajeevi, G. (2012). Study of ballast fouling in railway track formations. *Indian Geotechnical Journal*, 42(2), 87-99. http://doi.org/10.1007/s40098-012-0006-6.

Anderson, W.F., & Fair, P. (2008). Behavior of railroad ballast under monotonic and cyclic loading. *Journal of Geotechnical and Geoenvironmental Engineering*, 134(3), 316-327. http://doi.org/10.1061/(ASCE)1090-0241(2008)134:3(316).

ASTM D5311. (2011). *Standard test method for load controlled cyclic triaxial strength of soil*. ASTM International, West Conshohocken, PA.

ASTM C127. (2015). *Standard test method for relative density (specific gravity) and absorption of coarse aggregate*. ASTM International, West Conshohocken, PA.

ASTM D6918. (2017). *Standard test method for resistance of coarse aggregate to degradation by abrasion in the micro-deval apparatus*. ASTM International, West Conshohocken, PA.

ASTM C1856. (2024). *Standard practice for fabricating and testing specimens of ultra-high performance concrete*. ASTM International, West Conshohocken, PA.

Brown, S.F., Kwan, J., & Thom, N.H. (2007). Identifying the key parameters that influence geogrid reinforcement of railway ballast. *Geotextiles and Geomembranes*, 25(6), 326-335. http://doi.org/10.1016/j.geotexmem.2007.06.003.

Cazzuffi, D., Venesla, S., Rinaldi, M., & Zocca, M. (1986). The mechanical properties of geotextiles: Italian standard and interlaboratory test comparison. In *Proceedings of 3rd International Conference on Geotextiles* (pp. 695-700), Vienna, Austria.

Chen, Q., Abu-Farsakh, M., Voyiadjis, G.Z., & Souci, G. (2013). Shakedown analysis of geogrid-reinforced granular base material. *Journal of Materials in Civil Engineering*, 25(3), 337-346. http://doi.org/10.1061/(ASCE)MT.1943-5533.0000601.

Conceição, K.S., Maia, P.C.A., & Cordeiro, G.C. (2022). Use of ultra-high-performance concrete to produce standard coarse aggregates. *Journal of Testing and Evaluation*, 50(2), 1224-1235. http://doi.org/10.1520/JTE20210013.

Delgado, B.G., Fonseca, A.V., Fortunato, E., & Maia, P. (2019). Mechanical behavior of inert steel slag ballast for heavy haul rail track: laboratory evaluation. *Transportation Geotechnics*, 20, 100243. http://doi.org/10.1016/j.trgeo.2019.100243.

Desbrousses, R.L.E., Meguid, M.A., & Bhat, S. (2023). Experimental investigation of the effects of subgrade strength and geogrid location on the cyclic response of geogrid-reinforced ballast. *International Journal of Geosynthetics and Ground Engineering*, 9(6), 67. http://doi.org/10.1007/s40891-023-00486-3.

EN 13286-7. (2004). *Unbound and hydraulically bound mixtures - part 7: cyclic load triaxial test for unbound mixtures.* CEN, Brussels.

Fernandes, G., Palmeira, E.M., & Gomes, R.C. (2008). Performance of geosynthetic reinforced alternative sub-ballast material in a railway track. *Geosynthetics International*, 15(5), 311-321. http://doi.org/10.1680/gein.2008.15.5.311.

Guo, Y., Markine, V., & Jing, G. (2021). Review of ballast track tamping: Mechanism, challenges and solutions. *Construction & Building Materials*, 300(20), 123940. http://doi.org/10.1016/j.conbuildmat.2021.123940.

Han, B., Ling, J., Shu, X., Gong, H., & Huang, B. (2018). Laboratory investigation of particle size effects on the shear behavior of aggregate-geogrid interface. *Construction & Building Materials*, 158, 1015-1025. http://doi.org/10.1016/j.conbuildmat.2017.10.045.

Huang, H., Tutumluer, E., & Dombrow, W. (2009). Laboratory characterization of fouled railroad ballast behavior. *Transportation Research Record: Journal of the Transportation Research Board*, 2117(1), 93-101. http://doi.org/10.3141/2117-12.

Hussaini, S.K.K. (2013). *An experimental study on the deformation behaviour of geosynthetically reinforced ballast* [Doctoral thesis, University of Wollongong]. University of Wollongong's repository. Retrieved in December 8, 2024, from https://ro.uow.edu.au/theses/3799/

Indraratna, B., Ionescu, D., & Christie, H.D. (1998). Shear behavior of railway ballast based on large-scale triaxial tests. *Journal of Geotechnical and Geoenvironmental Engineering*, 124(5), 439-449. http://doi.org/10.1061/(ASCE)1090-0241(1998)124:5(439).

Indraratna, B., & Salim, W. (2003). Deformation and degradation mechanics of recycled ballast stabilised with geosynthetics. *Soil and Foundation*, 43(4), 35-46. http://doi.org/10.3208/sandf.43.4_35.

Indraratna, B., Lackenby, J., & Christie, D. (2005). Effect of confining pressure on the degradation of ballast under cyclic loading. *Geotechnique*, 55(4), 325-328. http://doi.org/10.1680/geot.2005.55.4.325.

Indraratna, B., Khabbaz, H., Salim, W., & Christie, D. (2006). Geotechnical properties of ballast and the role of geosynthetics in rail track stabilisation. *Ground Improvement*, 10(3), 91-101. http://doi.org/10.1680/grim.2006.10.3.91.

Indraratna, B., Thakur, P.K., & Vinod, J.S. (2010). Experimental and numerical study of railway ballast behavior under cyclic loading. *International Journal of Geomechanics*, 10(4), 136-144. http://doi.org/10.1061/(ASCE)GM.1943-5622.0000055.

Indraratna, B., Hussaini, S.K.K., & Vinod, J.S. (2013). The lateral displacement response of geogrid-reinforced ballast under cyclic loading. *Geotextiles and Geomembranes*, 39(3), 20-29. http://doi.org/10.1016/j.geotexmem.2013.07.007.

Indraratna, B., Ngo, N.T., Rujikiatkamjorn, C., & Vinod, J.S. (2014). Behavior of fresh and fouled railway ballast subjected to direct shear testing: discrete element simulation. *International Journal of Geomechanics*, 14(1), 34-44. http://doi.org/10.1061/(ASCE)GM.1943-5622.0000264.

Jideani, T., & Gräbe, H. (2020). The development of suitable cyclic loading and boundary conditions for ballast box tests. *Journal of the South African Institution of Civil Engineering*, 61(4), 59-72. http://doi.org/10.17159/2309-8775/2019/v61n4a6.

Koohmishi, M., & Palassi, M. (2018). Effect of gradation of aggregate and size of fouling materials on hydraulic conductivity of sand-fouled railway ballast. *Construction & Building Materials*, 167, 514-523. http://doi.org/10.1016/j.conbuildmat.2018.02.040.

Lackenby, J., Indraratna, B., Mcdowell, G., & Christie, D. (2007). Effect of confining pressure on ballast degradation and deformation under cyclic triaxial loading. *Geotechnique*, 57(6), 527-536. http://doi.org/10.1680/geot.2007.57.6.527.

Lekarp, F., Isacsson, U., & Dawson, A. (2000). State of the art. II: permanent strain response of unbound aggregates. *Journal of Transportation Engineering*, 126(1), 76-83. http://doi.org/10.1061/(ASCE)0733-947X(2000)126:1(76).

Liu, S., Huang, H., Qiu, T., & Kwon, J. (2016). Effect of geogrid on railroad ballast particle movement. *Transportation Geotechnics*, 9, 110-122. http://doi.org/10.1016/j.trgeo.2016.08.003.

Marsal, R.J. (1967). Large scale testing of rockfill materials. *Journal of the Soil Mechanics and Foundations Division*, 93(2), 23-47. http://doi.org/10.1061/JSFEAQ.0000958.

McDowell, G.R., Harireche, O., Konietzky, H., Brown, S.F., & Thom, N.H. (2006). Discrete element modelling of geogrid-reinforced aggregates. *Geotechnical Engineering*, 159(1), 35-48. http://doi.org/10.1680/geng.2006.159.1.35.

Merheb, A.H.M., Motta, R., Bernucci, L., Moura, E., Costa, R., Vieira, T., & Sgavioli, F. (2014). Equipamento triaxial cíclico de grande escala para análise mecânica de lastro ferroviário. *Transportes*, 22(3), 53-63. http://doi.org/10.14295/transportes.v22i3.804.

Palmeira, E.M., Gardoni, M.D.G., & Araújo, G.L.S. (2021). Geossintéticos em engenharia geotécnica e geoambiental: avanços e perspectivas. *Geotecnia*, 152(152), 337-368. http://doi.org/10.14195/2184-8394_152_10.

Qian, Y., Tutumluer, E., Mishra, D., & Kazmee, H. (2018). Triaxial testing and discrete element modelling of geogrid-stabilised rail ballast. *Proceedings of the Institution of Civil Engineers: Ground Improvement*, 171(4), 223-231. http://doi.org/10.1680/jgrim.17.00068.

Sgavioli, F., Bernucci, L., Costa, R., Motta, R., & Moura, E. (2015). Análise do custo do ciclo de vida do lastro ferroviário na estrada de ferro Vitória Minas. *Transportes*, 23(2), 5-12. http://doi.org/10.14295/transportes.v23i4.981.

Shi, C., Fan, Z., Connolly, D.P., Jing, G., Markine, V., & Guo, Y. (2023). Railway ballast performance: recent advances in the understanding of geometry, distribution and degradation. *Transportation Geotechnics*, 41, 101042. http://doi.org/10.1016/j.trgeo.2023.101042.

Shi, X. (2009). *Prediction of permanent deformation in railway track* [Doctoral thesis]. University of Nottingham's repository.

Shukla, S.K., Sivakugan, N., & Das, B.M. (2009). Fundamental concepts of soil reinforcement: an overview. *International Journal of Geotechnical Engineering*, 3(3), 329-342. http://doi.org/10.3328/IJGE.2009.03.03.329-342.

Skoglund, K.A. (2002). *A study of some factors in mechanistic railway track design* [Doctoral thesis, Norwegian University of Science and Technology]. Norwegian University of Science and Technology's repository. Retrieved in December 8, 2024, from http://hdl.handle.net/11250/231131

Suiker, A.S.J., Selig, E.T., & Frenkel, R. (2005). Static and cyclic triaxial testing of ballast and subballast. *Journal of Geotechnical and Geoenvironmental Engineering*, 131(6), 771-782. http://doi.org/10.1061/(ASCE)1090-0241(2005)131:6(771).

Sun, Q.D., Indraratna, B., & Nimbalkar, S. (2016). Deformation and degradation mechanisms of railway ballast under high frequency cyclic loading. *Journal of Geotechnical and Geoenvironmental Engineering*, 142(1), 04015056. http://doi.org/10.1061/(ASCE)GT.1943-5606.0001375.

Sweta, K., & Hussaini, S.K.K. (2020). Effect of geogrid on deformation response and resilient modulus of railroad ballast under cyclic loading. *Construction & Building Materials*, 264, 120690. http://doi.org/10.1016/j.conbuildmat.2020.120690.

Tutumluer, E., Huang, H., & Bian, X. (2009). Research on the behavior of geogrids in stabilization applications. In *Proceedings of the Jubilee Symposium on Polymer Geogrid Reinforcement*, London, UK.

Viswanadham, B.V.S., & König, D. (2004). Studies on scaling and instrumentation of a geogrid. *Geotextiles and Geomembranes*, 22(5), 307-328. http://doi.org/10.1016/S0266-1144(03)00045-1.

Werkmeister, S., Dawson, A.R., & Wellner, F. (2001). Permanent deformation behavior of granular materials and the shakedown concept. *Transportation Research Record: Journal of the Transportation Research Board*, 1757(1), 75-81. http://doi.org/10.3141/1757-09.

Zhang, X., Zhao, C., & Zhai, W. (2019). Importance of load frequency in applying cyclic loads to investigate ballast deformation under high-speed train loads. *Soil Dynamics and Earthquake Engineering*, 120, 28-38. http://doi.org/10.1016/j.soildyn.2019.01.023.

Soil. Rocks, São Paulo, 2025 48(2):e2025008924

11